Leaky Mode Analysis of Microstrip Transmission Lines with EFIE Method

by

Ching-Her Lee*

Abstract

There has recently been a resurgence of interest in the propagation characteristics of open integrated microstrip transmission lines. This is due to the discovery of leaky regimes for higher-order modes on the lines. In contrast to the dominant EH_0 mode on microstrip transmission lines, three distinct propagation regimes for higher-order modes exist on open integrated microstrip transmission lines. In this paper a powerful, new integral equation formulation is used to analyze propagation in all three regimes for integrated microstrip transmission lines. This formulation provides a clear physical picture of the different propagation regimes based on the location of surface wave poles and branch points in the complex spectral variable plane. The integral equation is discretized via the method of moments, where entire-domain basis functions incorporating suitable edge behavior are utilized to provide

* Associate professor, Department of Industrial Education, National Changhua University of Education.

convergence with relatively few terms. Results obtained in the form of propagation constants and current distributions are compared with the results of other workers, and good agreement is observed.

KEY WORDS: Microstrip transmission line, EFIE, Leaky mode, propagation regimes.

Leaky Mode Analysis of Microstrip Transmission Lines with EFIE Method

I. INTRODUCTION

In the past few years, there has been a resurgence of interest in the propagation characteristics of open integrated microstrip transmission lines. This is in large part due to the discovery of leaky regimes for higher-order modes on the lines. In contrast to the dominant EH_0 mode on microstrip transmission lines, three distinct propagation regimes for higher-order modes exist on open integrated microstrip transmission lines. One such work was first published by Ermert [1] for closed microstrip structures. He presented a thorough mode-matching analysis of the fundamental and the first two higher order modes. A principal conclusion from his work was that a "radiation" region exists close to the cutoff of these modes. However, Ermert's description was incomplete, and due to the exponentially growing nature of these leaky modes, he rejected any inclusion of such modes in his analysis. Later Oliner [2] and Oliner and Lee [3, 4] and Michalski and Zheng [5, 6], described three distinct propagation regimes for higher-order modes on open integrated microstrip transmission lines. These works help to clarify the unclear features hidden in the leaky modes.

The first regime, denoted here as the bound regime, is characterized by propagation constants that are purely real (in the low loss limit) and fields that are confined to the vicinity of the transmission line. The dominant EH_0 mode of open microstrip structures is always in this regime. The second propagation regime, the surface wave regime, is characterized by complex propagation constants with relatively small imaginary parts, resulting in attenuation of the signal traversing the line. This attenuation is due to the fact that surface waves traveling away from the axis of the transmission line are excited in the film layer of the integrated circuit background structure, and energy from the transmission line mode is transferred to these surface waves. The third propagation regime, the radiation regime, is characterized by complex propagation constants with relatively large imaginary parts. In this case losses occur from both excitation of surface waves in the film layer and radiation into the cover

medium surrounding the integrated microstrip transmission line. Microstrip modes operated in the last two regimes are called leaky modes. The existence of such leakage phenomena has been experimentally verified by Shigesawa, et. al., in the closely related case of integrated dielectric waveguides [7].

In this paper a powerful, newly developed electric field integral equation [8] is used to analyze propagation in all three regimes for integrated microstrip transmission lines. This formulation provides a clear physical picture of the different propagation regimes based on the location of surface wave poles and branch points in the complex spectral variable plane. The integral equation is discretized via the method of moments, where entire-domain basis functions incorporating suitable edge behavior are utilized to provide convergence with relatively few terms. The results obtained are compared with the results of Oliner [2] and Michalski and Zheng [5, 6], and good agreement is observed.

In Section II the integral equation formulation is introduced. Based on the definition of parameters in the formulation, the three above mentioned propagation regimes are identified and discussed in Section III. Section IV details the application of the method of moments of the integral equation and discusses numerical implementation of results. In Section V we present numerical results in the form of dispersion curves and current distributions in all three propagation regimes. As a check, these results are compared to those obtained by Oliner [2] and Michalski and Zheng [5, 6]. We close in Section VI with a discussion of further applicability of these techniques in analysis of coupled microstrip transmission lines and isolated and coupled integrated dielectric waveguides.

II. FORMULATION

Consider the integrated microstrip transmission line geometry depicted in Figure 1. The integral equation satisfied by the unknown surface current on the line with an assumed propagation dependence of exp[j(ωt - ζz)] is derived in [8, 9]:

$$\hat{t}\cdot(k_c^2+\tilde{\nabla}\tilde{\nabla}\cdot)\int_\ell \overleftrightarrow{g}(\vec{\rho}\mid\vec{\rho}';\zeta)\cdot\vec{k}(\vec{\rho}';\zeta)\,d\ell'=0,\quad \vec{\rho}\in\ell \tag{1}$$

where $\vec{k}(\vec{\rho}';\zeta)$ is the unknown surface current on the microstrip line, $\hat{t}$ is a unit tangent to the microstrip line surface and $\tilde{\nabla}=\nabla_t+j\zeta\hat{z}=\hat{x}\frac{\partial}{\partial x}+\hat{y}\frac{\partial}{\partial y}+j\zeta\hat{z}$ is the axially transformed del operator . We have assumed that the natural microstrip modes are of main interest.

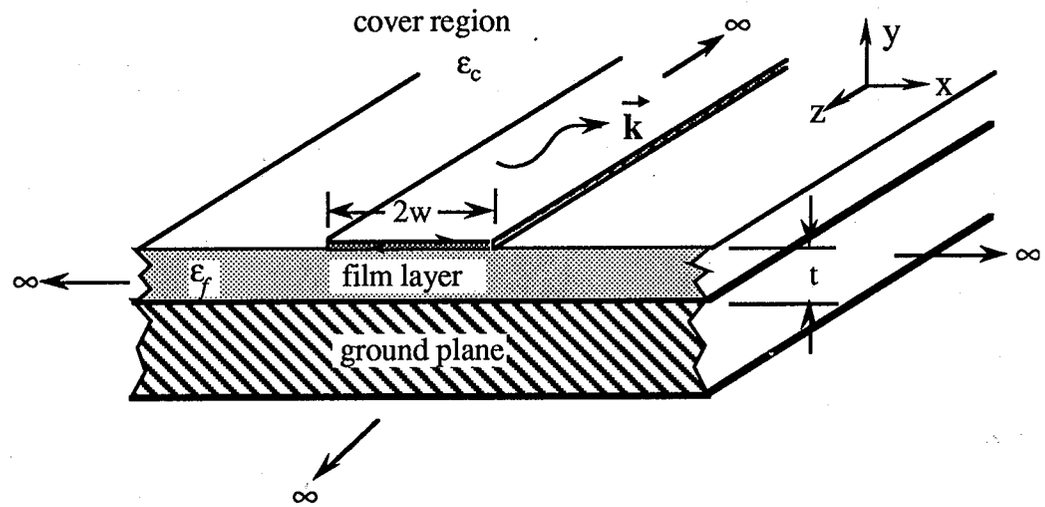

Fig. 1 An axially uniform, isolated microstrip transmission line.

The electric Hertzian potential Green's dyad decomposes into a principal and a reflected part, $\overleftrightarrow{g}(\vec{\rho}\mid\vec{\rho}';\zeta)=\overleftrightarrow{g}^p+\overleftrightarrow{g}^r$, where $\overleftrightarrow{g}^p$ is the two-dimensional unbounded space Green's function in integral form, and the reflected Green's function has components

$$\overleftrightarrow{g}^r(\vec{\rho}\mid\vec{\rho}';\zeta)=\hat{x}g_t^r\hat{x}+\hat{y}\left(\frac{\partial}{\partial x}g_c^r\hat{x}+g_n^r\hat{y}+j\zeta g_c^r\hat{z}\right)+\hat{z}g_t^r\hat{z}$$

The scalar components of the principal and reflected Green's dyads take the following forms [9]:

$$g^p(\vec{\rho}\mid\vec{\rho}';\zeta)=\int_{-\infty}^{\infty}\frac{e^{j\xi(x-x')}e^{-p_c|y-y'|}}{4\pi p_c}\,d\xi \tag{2a}$$

$$\begin{pmatrix} g_t^r \\ g_n^r \\ g_c^r \end{pmatrix} = \int_{-\infty}^{\infty} \begin{pmatrix} R_t(\lambda) \\ R_n(\lambda) \\ C(\lambda) \end{pmatrix} \frac{e^{j\xi(x-x')} e^{-p_c(y+y')}}{4\pi p_c} d\xi \tag{2b}$$

where $\lambda^2 = \xi^2 + \zeta^2$. The wavenumber parameters are defined by $p_{c,f}^2 = \xi^2 + \zeta^2 - k_{c,f}^2$, and k_c and k_f are the wavenumbers in the cover region and film layer, respectively. The reflection and coupling coefficients in the integrands of the reflected Green's dyad components are given by

$$R_t = \frac{p_c - p_f \coth(p_f t)}{p_c + p_f \coth(p_f t)}, \qquad R_n = \frac{K p_c - p_f \tanh(p_f t)}{K p_c + p_f \tanh(p_f t)}$$

$$C = \frac{2(K-1)p_c}{[p_c + p_f \coth(p_f t)]\,[K p_c + p_f \tanh(p_f t)]}, \qquad K = \frac{\varepsilon_f}{\varepsilon_c}$$

where ε_c and ε_f are the permittivities of the cover and film regions.

For Eq.(1) to be applied in the following work, we simplify it further by assuming that the microstrip line in Fig. 1 is thin and of negligible thickness. In this case, the induced surface current is on the y' = 0 plane and the contour ℓ involved in the integration becomes a line segment extending in x direction. For the specialized structure, the tangential unit vector $\hat{t}$ and the surface current $\vec{k}$ can be expressed as

$$\hat{t} = \hat{x} t_x + \hat{z} t_z, \quad \vec{k} = \hat{x} k_x + \hat{z} k_z$$

To evaluate Eq.(1), we rewrite the integral representations of the scalar components g^p and $g_{t,n,c}^r$ as

$$g_{t,n,c}^{p,r}(\vec{\rho}\,|\,x';\zeta) = \int_{-\infty}^{\infty} i_{t,n,c}^{p,r}(\vec{\rho}\,|\,x';\zeta,\xi)\, d\xi \tag{3}$$

with

$$i^p = \frac{e^{j\xi(x-x')} e^{-p_c|y|}}{4\pi p_c}$$

$$\begin{pmatrix} i_t^r \\ i_n^r \\ i_c^r \end{pmatrix} = \begin{pmatrix} R_t \\ R_n \\ C \end{pmatrix} \frac{e^{j\xi(x-x')} e^{-p_c y}}{4\pi p_c}$$

where the fact y' = 0 has been applied. Substitution of (3) into Eq.(1) gives

$$\hat{t} \cdot \lim_{y \to 0} \int_{\ell_x} \int_{-\infty}^{\infty} (k_c^2 + \tilde{\tilde{\nabla}}\tilde{\tilde{\nabla}} \cdot)\, \vec{i}(\vec{\rho}\,|\,x';\zeta,\xi) \cdot \vec{k}(x';\zeta)\, d\xi\, dx' = 0 \tag{4}$$

where we have assumed interchange of differentiation and integration is valid. Notice that the operator $\tilde{\tilde{\nabla}}$ now becomes $\tilde{\tilde{\nabla}} = j\xi\hat{x} + \frac{\partial}{\partial y}\hat{y} + j\zeta\hat{z}$ since $\frac{\partial}{\partial x} \to j\xi$ when we interchange $\frac{\partial}{\partial x}$ and $\int d\xi$.

It is seen that a discontinuity at y = 0 will be encountered while taking derivative of the quantity i^p on y. In solving Eq.(4), we must exercise caution in taking the limit as $y \to 0$ because of the derivatives on y involved in $\tilde{\tilde{\nabla}}$ operation. By omitting some purely algebraic steps, we obtain

$$\vec{i} \cdot \vec{k} = (i^p + i_t^r)(\hat{x} k_x + \hat{z} k_z) + \hat{y} i_c^r (j\xi k_x + j\zeta k_z) \tag{5}$$

so that

$$\hat{t} \cdot \vec{i} \cdot \vec{k} = (i^p + i_t^r)(t_x k_x + t_z k_z) \tag{6}$$

Which poses no problem in the limit as $y \to 0$. Also

$$\tilde{\tilde{\nabla}} \cdot \vec{i} \cdot \vec{k} = (j\xi\hat{x} + \frac{\partial}{\partial y}\hat{y} + j\zeta\hat{z}) \cdot [(i^p + i_t^r)(\hat{x} k_x + \hat{z} k_z) + \hat{y} i_c^r (j\xi k_x + j\zeta k_z)] \tag{7}$$

which gives

$$\tilde{\tilde{\nabla}} \cdot \vec{i} \cdot \vec{k} = (i^p + i_t^r)(j\xi k_x + j\zeta k_z) - p_c i_c^r (j\xi k_x + j\zeta k_z)] \tag{8}$$

where $\frac{\partial}{\partial y}\,\mathbf{i}_c^r = -\,p_c\,\mathbf{i}_c^r$ has been applied. It is seen that $\frac{\partial}{\partial y}\hat{y}\cdot\mathbf{i}^p\mathbf{k}_x\hat{x} = 0$ and the derivative of $\mathbf{i}^p$ on y is not necessary to be calculated. This allows us to avoid getting into trouble while taking the limit $y \to 0$. We then obtain

$$\hat{t}\cdot\tilde{\tilde{\nabla}}\tilde{\tilde{\nabla}}\cdot\vec{i}\cdot\vec{k} = (j\xi t_x + j\zeta t_z)[(\mathbf{i}^p + \mathbf{i}_t^r)(j\xi\mathbf{k}_x + j\zeta\mathbf{k}_z) - p_c\mathbf{i}_c^r(j\xi\mathbf{k}_x + j\zeta\mathbf{k}_z)] \qquad (9)$$

Again the limit as $y \to 0$ poses no problem. Substituting (6) and (9) into Eq.(4) and noting that when $y = 0$ the quantities $\mathbf{i}^p$, $\mathbf{i}_t^r$ and $\mathbf{i}_c^r$ become

$$\mathbf{i}^p = \frac{e^{j\xi(x-x')}}{4\pi p_c}$$

$$\begin{Bmatrix}\mathbf{i}_t^r\\ \mathbf{i}_c^r\end{Bmatrix} = \begin{Bmatrix}R_t\\ C\end{Bmatrix}\frac{e^{j\xi(x-x')}}{4\pi p_c} \qquad (10)$$

respectively, we obtain, after taking the limit $y \to 0$ in the results, the integral equation as:

$$\int_{\ell_x}\int_{-\infty}^{\infty}\frac{e^{j\xi(x-x')}}{4\pi p_c}[k_c^2(1+R_t)(t_x\mathbf{k}_x + t_z\mathbf{k}_z) - (1+R_t-p_cC)(\xi t_x+\zeta t_z)(\xi\mathbf{k}_x+\zeta\mathbf{k}_z)]d\xi\,dx' = 0 \qquad (11)$$

Eventually, two coupled integral equations are obtained by letting $\hat{t} = \hat{x}$ and $\hat{t} = \hat{z}$. They are

$$\hat{x}: \int_{\ell_x}\int_{-\infty}^{\infty}\frac{e^{j\xi(x-x')}}{4\pi p_c}[\,k_c^2(1+R_t)\mathbf{k}_x - \xi(1+R_t-p_cC)(\xi\mathbf{k}_x+\zeta\mathbf{k}_z)]\,d\xi\,dx' = 0 \qquad (12a)$$

$$\hat{z}: \int_{\ell_x}\int_{-\infty}^{\infty}\frac{e^{j\xi(x-x')}}{4\pi p_c}[\,k_c^2(1+R_t)\mathbf{k}_z - \zeta(1+R_t-p_cC)(\xi\mathbf{k}_x+\zeta\mathbf{k}_z)]\,d\xi\,dx' = 0 \qquad (12b)$$

Equations (12) are the final form of the electric field integral equations for thin isolated microstrip line to be used in Section IV.

III. PROPAGATION REGIMES

The integrands in the spectral representation of Green's dyad components contain multi-valued parameters p_c and p_f, necessitating a choice of branch cuts in the complex ξ plane. The integrands of the reflected Green's dyad also contain the coefficients R_t, R_n, and C. The first of which has a simple pole when $\lambda = \lambda_p$ is an eigenvalue of a TE mode of the symmetric slab background structure, the second of which has a simple pole when $\lambda = \lambda_p$ is an eigenvalue of a TM mode of the symmetric slab background structure, and the third of which has simple poles at both TE and TM eigenvalues. Careful examination of the integrands reveals that all are even functions of p_f, so the branch cut for this parameter is not implicated.

To correctly locate the positions of the poles and branch points in the complex ξ plane it is necessary to invoke material losses, and later take the low-loss limiting case. To this end we assume

$$\varepsilon_c = \varepsilon_c' - j\varepsilon_c'', \quad \varepsilon_f = \varepsilon_f' - j\varepsilon_f'', \qquad \varepsilon_c'',\ \varepsilon_f'' > 0$$

so that

$$k_c = k_{cr} - jk_{ci}, \quad \lambda_p = \lambda_{pr} - j\lambda_{pi}, \quad \zeta = \beta - j\alpha$$

where all quantities above are non-negative. Surface wave poles occur in the complex ξ plane at values of ξ which satisfy $\xi_p^2 + \zeta^2 = \lambda_p^2$, giving

$$\xi_p^2 = (\lambda_{pr}^2 - \lambda_{pi}^2 - \beta^2 + \alpha^2) - 2j(\lambda_{pr}\lambda_{pi} - \beta\alpha)$$

We will assume for convenience that the integrated circuit background structure supports only one surface wave, the dominant TM_0 mode, in frequency ranges of interest (a

restriction that will be removed later in sections IV and V). Similarly, the branch point in the complex ξ plane corresponding to p_c occurs when $\xi_b^2+\zeta^2-k_c^2=0$, or

$$\xi_b^2=(k_{cr}^2-k_{ci}^2-\beta^2+\alpha^2)-2j(k_{cr}k_{ci}-\beta\alpha)$$

Now consider the case of $\beta^2-\alpha^2 > \lambda_{pr}^2-\lambda_{pi}^2 > k_{cr}^2-k_{ci}^2$. This corresponds to pure guided microstrip mode in the bound regime. We first assume that material losses dominate, so $\lambda_{pr}\lambda_{pi} > \beta\alpha$, and then gradually allow propagation losses to increase (or equivalently, take the low loss limit) such that $\beta\alpha$ is greater than $\lambda_{pr}\lambda_{pi}$ and $k_{cr}k_{ci}$. This leads to a migration of the location of the surface wave pole and branch point in the complex ξ plane, as shown in Figure 2. Note that the migration of the pole and branch point do not cause them to cross the contour of integration, which is the real ξ axis. Thus in the bound regime, characterized by $\beta^2-\alpha^2 > \lambda_{pr}^2-\lambda_{pi}^2 > k_{cr}^2-k_{ci}^2$, evaluation of the spectral integrals in the expressions for the Green's dyad components can be performed in a straight-forward fashion.

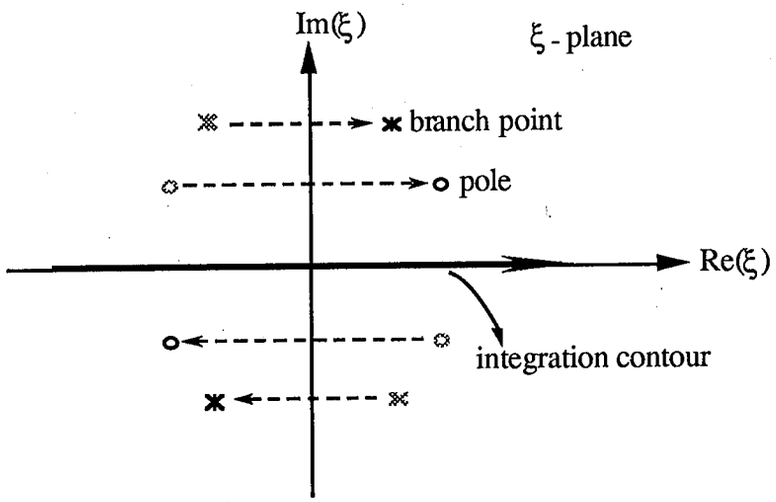

Fig. 2. Integration contour and migration paths of poles and branch points for bound regime.

Next consider the case of $\lambda_{pr}^2-\lambda_{pi}^2 > \beta^2-\alpha^2 > k_{cr}^2-k_{ci}^2$, which corresponds to the surface wave propagation regime. Again assuming material losses dominate and then

gradually allowing propagation losses to increase (or taking the low loss limit) until $\beta\alpha$ is greater than $\lambda_{pr}\lambda_{pi}$ and $k_{cr}k_{ci}$ we obtain the complex ξ plane picture of Figure 3. Note that in this case the surface wave pole has migrated across the contour of integration. Since the physical situation has not been altered, the integration contour should stay on the same side of the surface wave pole, as described by Boukamp and Jansen [10]. This necessitates detouring around the pole as shown in Figure 3, resulting in the inclusion of a residue term in evaluation of the spectral integral. This residue contribution corresponds to the surface wave which has been excited in the integrated circuit background structure, resulting in a decay in the microstrip transmission line mode ($\alpha > 0$). This surface wave travels in the integrated circuit surround at an angle to the microstrip axis with cosine β / λ_{pr}.

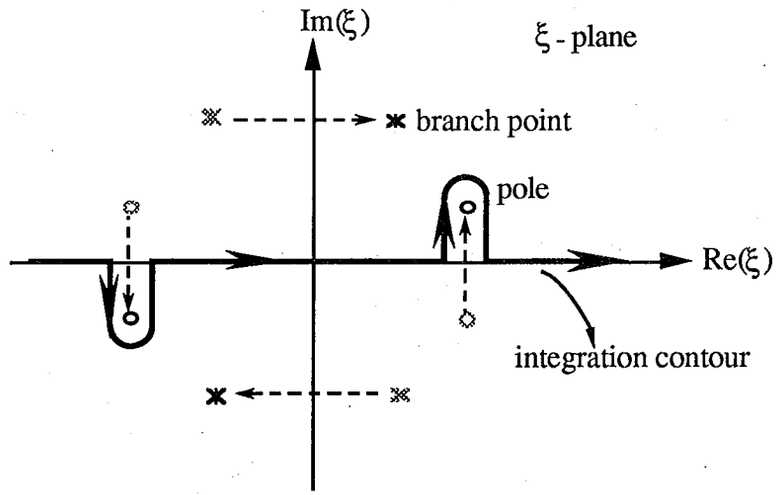

Fig. 3. Integration contour and migration paths for surface wave regime (or leaky regime (1) in Fig. 5).

The third propagation regime, the radiation regime, occurs when $\beta^2-\alpha^2 < k_{cr}^2-k_{ci}^2$. Allowing material losses to dominate and then gradually increasing propagation losses (or invoking the low-loss limit) until $\beta\alpha$ is-greater than $\lambda_{pr}\lambda_{pi}$ and $k_{cr}k_{ci}$ results in both the pole and the branch point migrating across the contour of integration, in a similar fashion as in Assailly, et. al. [11]. This effect is shown in Fig.4. For the same reasons given above, this necessitates deforming the contour of integration around the branch cut

and the surface wave pole as shown in the Figure. In this case propagation losses are quite large, since both radiation into the cover medium and surface waves in the film layer are excited.

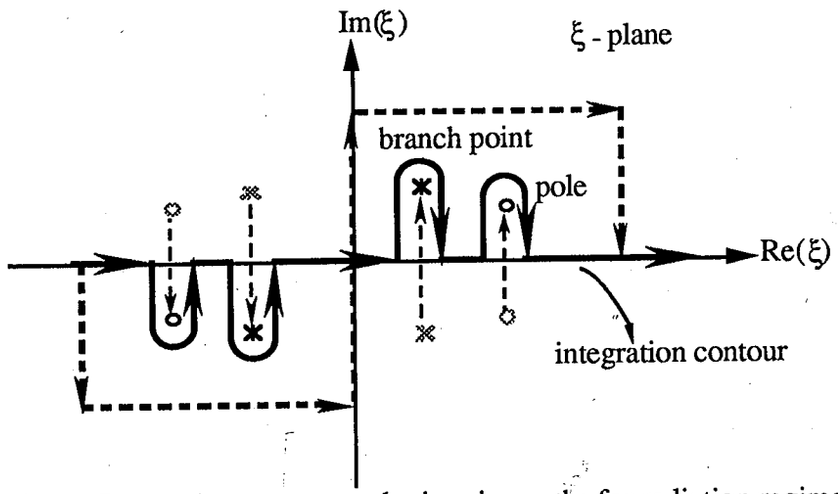

Fig. 4. Integration contour and migration paths for radiation regime (or leaky regime (2) in Fig. 5).

From the above discussion, we end up with three propagation regimes as:

$$\begin{aligned} \beta > \lambda_p, &\quad \text{bound regime} \\ k_c^2 < \beta^2 - \alpha^2 < \lambda_p^2, &\quad \text{surface wave regime} \\ \beta^2 - \alpha^2 < k_c^2, &\quad \text{radiation regime} \end{aligned} \tag{13}$$

where material losses in the film layer and in the cover medium have been assumed to be zero, and hence λ_p and k_c are purely real. A dispersion curve indicating the three propagation regimes is provided in Fig. 5.

IV. METHOD OF MOMENTS SOLUTION

To solve equation (1) numerically, let $\hat{t} = \hat{x}t_x + \hat{z}t_z$, and $\vec{k} = \hat{x}k_x + \hat{z}k_z$. We then follow a similar procedure as done in [12] by expanding $\mathbf{k}_x(x')$ and $\mathbf{k}_z(x')$ for even case (even $\mathbf{k}_z(x')$ and odd $\mathbf{k}_x(x')$) as follows

$$\mathbf{k}_x(x') \cong \sqrt{1-\left(\frac{x'}{w}\right)^2} \sum_{n=0}^{N-1} a_n\, U_{2n+1}\left(\frac{x'}{w}\right) \tag{14a}$$

$$\mathbf{k}_z(x') \cong \frac{1}{\sqrt{1-\left(\frac{x'}{w}\right)^2}} \sum_{n=0}^{N-1} b_n\, T_{2n}\left(\frac{x'}{w}\right) \tag{14b}$$

where a_n and b_n are expansion coefficients representing the contribution of each order of Chebyshev polynomials $U_n(x')$ and $T_n(x')$ to the unknown surface currents and the factors in front of the summation terms give $U_n(x')$ and $T_n(x')$ the correct edge behavior. For the expansion of currents of odd case (odd $\mathbf{k}_z(x')$ and even $\mathbf{k}_x(x')$), the same kinds of functions can still be used but with $U_{2n+1}(x')$ and $T_{2n}(x')$ replaced by $U_{2n}(x')$ and $T_{2n+1}(x')$, respectively. Notice that owing to even or odd symmetry of the currents, only even or odd orders of Chebyshev polynomials were used. The same functions were used later to test the equations in the longitudinal and transverse directions (Galerkin's method). After an usual MoM procedure, we finally obtain the I.E.'s for the open microstrip geometry as

Even case:

$$\begin{aligned} \hat{x}: &\sum_{n=0}^{N-1} a_n (-1)^n (n+1) \int_0^\infty \frac{\left[k_c^2 R - \xi^2 (R - C')\right]}{p_c \xi^2} J_{2n+2}(w\xi)\, J_{2m+2}(w\xi)\, d\xi \\ &- j \sum_{n=0}^{N-1} b_n (-1)^n \frac{w}{2} \zeta \int_0^\infty \frac{(R - C')}{p_c} J_{2n}(w\xi)\, J_{2m+2}(w\xi)\, d\xi = 0 \end{aligned} \tag{15a}$$

$$m = 0, 1, 2, \ldots, N-1.$$

$$\begin{aligned} \hat{z}: &\sum_{n=0}^{N-1} a_n (-1)^n (n+1)\, \zeta \int_0^\infty \frac{(R - C')}{p_c} J_{2n+2}(w\xi)\, J_{2m}(w\xi)\, d\xi \\ &- j \sum_{n=0}^{N-1} b_n (-1)^n \frac{w}{2} \int_0^\infty \frac{\left[k_c^2 R - \zeta^2 (R - C')\right]}{p_c} J_{2n}(w\xi)\, J_{2m}(w\xi)\, d\xi = 0 \end{aligned} \tag{15b}$$

Odd case:

$$\hat{x}: \sum_{n=0}^{N-1} a_n (-1)^n (n+1/2) \int_0^\infty \frac{\left[k_c^2 R - \xi^2 (R - C')\right]}{p_c \xi^2} J_{2n+1}(w\xi) J_{2m+1}(w\xi)\, d\xi$$

$$+ j \sum_{n=0}^{N-1} b_n (-1)^n \frac{w}{2} \zeta \int_0^\infty \frac{(R - C')}{p_c} J_{2n+1}(w\xi) J_{2m+1}(w\xi)\, d\xi = 0 \qquad (16a)$$

$$m = 0, 1, 2, \ldots, N-1$$

$$\hat{z}: \sum_{n=0}^{N-1} a_n (-1)^n (n+1/2) \zeta \int_0^\infty \frac{(R - C')}{p_c} J_{2n+1}(w\xi) J_{2m+1}(w\xi)\, d\xi$$

$$+ j \sum_{n=0}^{N-1} b_n (-1)^n \frac{w}{2} \int_0^\infty \frac{\left[k_c^2 R - \zeta^2 (R - C')\right]}{p_c} J_{2n+1}(w\xi) J_{2m+1}(w\xi)\, d\xi = 0 \qquad (16b)$$

where $R = 1+R_t$ and $C' = p_c C$.

This is a homogeneous system of 2N simultaneous algebraic equations for the 2N current expansion coefficients, It has nontrivial solution for those values of ζ which render its determinant vanish. To obtain the propagation constants of various modes, we can iterate, using Müller's method, to search for the zeros of the determinant in the complex ζ plane. In the bound regime, the zeros are purely real (α=0), which belong to bound modes; however, in the leaky regime, the zeros are complex ($\zeta = \beta - j\alpha$), and correspond to leaky modes.

Numerically, in evaluating the infinite integrals, a path along the dashed line shown in Figure 4 should be chosen whenever a surface wave pole near (or right on) the real ξ-axis is encountered to avoid the numerical difficulty, since at that point the integrand is nearly singular (or singular). Also note that in regime 3, on performing the integration along the real ξ-axis in the interval [0, ξ_b] (where the contribution of the radiation comes from), the wavenumber parameter p_c which involves a square root operation has to be negated if an intrinsic function (in a computer program) which takes the principal value of a square root is used. Due to the branch cut, the angle chosen for p_c is 180° different from its principal value.

Typical calculated results including dispersion curves and current distributions are shown in next section and, wherever possible, are compared to other researchers' work.

V. NUMERICAL RESULTS

In Figure 6, we present the dispersion curves of the first three higher order modes (EH_1, EH_2 and EH_3) in their leaky regime for an open microstrip line geometry depicted in Fig. 1. The same structure was previously analyzed by Oliner [2] using an approximate, asymptotic approach [13], and also by Michalski and Zheng [6, 14] utilizing a rigorous analysis based on the mixed-potential electric field integral equation (MPIE). Results from the three different approaches are seen to agree quite well for EH_1 mode; the agreement is somewhat less favorable for higher order modes.

In Figure 7, we show dispersion characteristics of the fundamental and first three higher order modes in both bound and leaky regimes for a narrower microstrip line with a higher dielectric constant. This microstrip geometry was previously analyzed by Ermert [1] and Lee and Bagby [15] in the bound regime and lately by Michalski and Zheng [6] in both the bound and leaky regimes. Our results for EH_0 and EH_1 modes are seen to agree completely with Michalski and Zheng's work; the agreement is also quite good for EH_2 mode. The dispersion curves TM_0 and TE_1 in this figure represent the first two surface wave modes supported by the symmetric slab waveguide (the dielectric layer and infinite conducting plane assembly). When β/k_0 crosses TM_0 line, the corresponding microstrip mode enters the leaky regime.

Figures 6 and 7 show that the leakage is large in lower frequency range, the leakage gradually decreases while the frequency moves up and ultimately becomes lossless after entering the bound regime where ζ is purely real ($\alpha = 0$).

In Figures 8, 9 and 10, we present some sample current distributions of the three higher order modes of the narrower microstrip. The numbers 1,3 and 2,4 represent the real and imaginary parts of currents corresponding to two different operating frequencies, respectively. Currents in each figure are normalized to have a maximum value of one. It is noted that there is relatively less change in the longitudinal current distribution than in the transverse current distribution as the microstrip mode passes from the bound regime to the leakage regime. Also notice that in the bound regime, the real part dominates the longitudinal current and the imaginary part dominates the

transverse current, which means the currents are 90° out of phase (as can easily be verified by the continuity equation). This is, however, not the case for leaky modes.

The same current distributions are supported in Michalski and Zheng's work [5, 6] using subdomain basis MoM. Comparison shows that the shape of currents are similar, whereas the values are quite different due to normalization and an opposite propagating direction being used in their work.

VI. CONCLUSIONS

In this paper a powerful, new integral equation formulation was used to analyze propagation in all three regimes for integrated microstrip transmission lines. This formulation provides a clear physical picture of the different propagation regimes based on the location of poles and branch points in the complex spectral variable plane. The integral equation was discretized via the method of moments, where entire-domain basis functions incorporating the correct edge behavior were utilized to provide improved accuracy and convergence with relatively few terms. The results obtained are in good agreement while compared with the results obtained by other techniques.

The first regime, denoted as the bound regime, is characterized by propagation constants which are purely real (in the low loss limit) and fields which are confined to the vicinity of the transmission line. The second propagation regime, the surface wave regime, is characterized by complex propagation constants with relatively small imaginary parts, resulting in attenuation of the signal traversing the line. This attenuation is due to the fact that surface waves traveling away from the axis of the transmission line are excited in the film layer of the integrated circuit background structure, and energy from the transmission line mode is transferred to these surface waves. The third propagation regime, the radiation regime, is characterized by complex propagation constants with relatively large imaginary parts. In this case losses occur from both excitation of surface waves in the film layer and from radiation into the cover medium surrounding the integrated microstrip transmission line.

We are now in the process of utilizing the results of these lossy modes to the design of microstrip device couplers, and extending this work to isolated and coupled integrated dielectric waveguides.

REFERENCES

[1] H. Ermert, "Guiding and radiation characteristics of planar waveguides," IEE Microwave, Optics, and Acoustics, vol. 3, Mar. 1979, pp. 59-62.

[2] A. A. Oliner, "Leakage from higher modes on microstrip line with application to antennas," Radio Sci., Vol. 22, No. 6, Nov. 1987, pp. 907-912.

[3] A. A. Oliner and K. S. Lee, "Microstrip leaky wave strip antennas," Digest of the AP-S Int. Symp., Philadelphia, PA, Aug. 1986, pp. 443-446.

[4] A. A. Oliner and K. S. Lee, "The nature of the leakage from higher modes on microstrip line," Digest of the MTT Int. Symp., 1986, pp. 57-60.

[5] K. A. Michalski and D. Zheng, "On the leaky modes of open microstrip lines," Microwave and Optical Tech. Lett., vol. 2, no. 1, Jan. 1989, pp. 6-8.

[6] K. A. Michalski and D. Zheng, "Rigorous analysis of open microstrip lines of arbitrary cross-section in bound and leaky regimes," IEEE Trans. Microwave Theory Tech., submitted.

[7] H. Shigesawa, M. Tauji, H. S. Myung, S. T. Peng, and A. A. Oliner, "Direct experimental confirmation of new leakage effects on open dielectric strip waveguides," Digest of the Int. MTT-S Symp., 1983, pp. 293-295.

[8] J. S. Bagby and D. P. Nyquist, "Dyadic Green's functions for integrated electronic and optical circuits," IEEE Trans. Microwave Theory Tech., vol. 35, no. 2, Feb. 1987, pp. 206-210.

[9] C.-H. Lee, Integral Equation Analysis of Microstrip Transmission Lines, Ph. D. Dissertation, The University of Texas at Arlington, 1989, Chap. 3.

[10] J. Boukamp and R. H. Jansen, "Spectral domain investigation of surface wave excitation and radiation by microstrip lines and microstrip disk resonators," Proc. of the European Microwave Conf., Sept. 1983, pp. 721-726.

[11] S. Assailly, C. Terret, J. P. Daniel, G. Besnier, J. Mosig, and B Roudot, "Spectral domain approach applied to open resonators: application to microstrip antennas," Electron. Lett., vol. 24, no. 2, Jan. 1988, pp. 105-106.

[12] J. S. Bagby, C.-H. Lee, Y. Yuan, and D. P. Nyquist, "Entire-domain basis MoM analysis of coupled microstrip transmission lines," IEEE Trans. Microwave Theory Tech., vol. 40, no. 1, Jan. 1992, pp.49-57.

[13] E. F. Kuester, R. G. Johnk, and D. C. Chang, "The thin-substrate approximation for reflection from the end of a slab-loaded parallel-plate waveguide with application to microstrip patch antennas", IEEE Trans. Antennas Propagat., vol. AP-30, Sept. 1982, pp. 910-917.

[14] K. A. Michalski and D. Zheng, "Rigorous analysis of open microstrip lines with finite thickness -- the mixed-potential integral equation approach," Digest of the URSI Nat. Radio Sci. meeting, Boulder, CO, Jan. 1989, p. 215.

[15] J. S. Bagby, C.-H. Lee, Y. Yuan, and D. P. Nyquist, "Entire-domain basis...," op. cit.

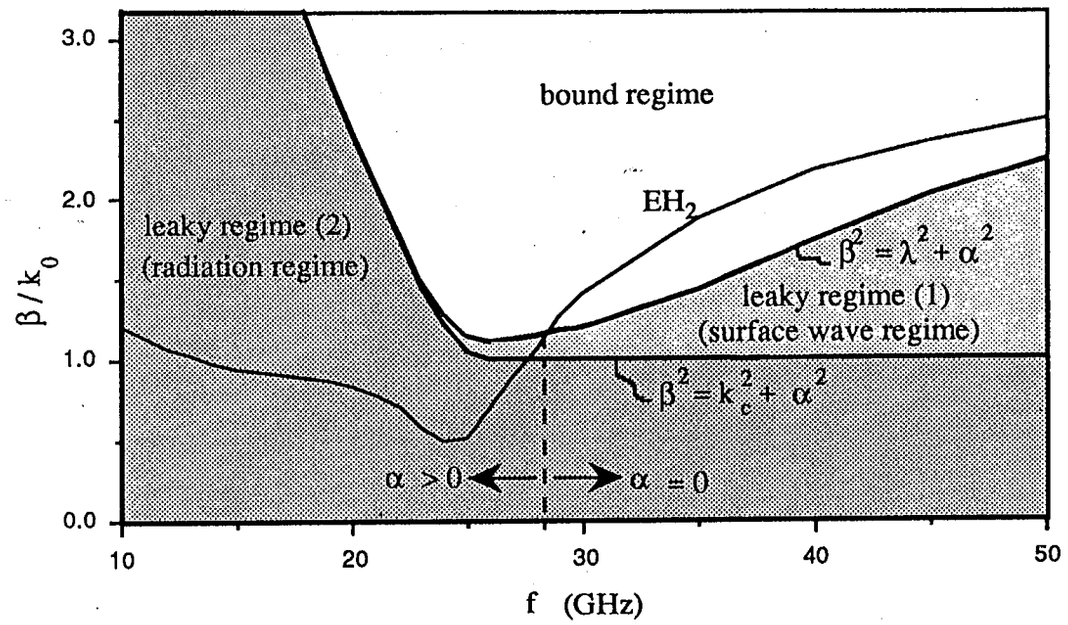

Fig. 5. Propagation regime diagram. The EH_2 mode is the second higher order mode of the microstrip shown in Fig. 1.

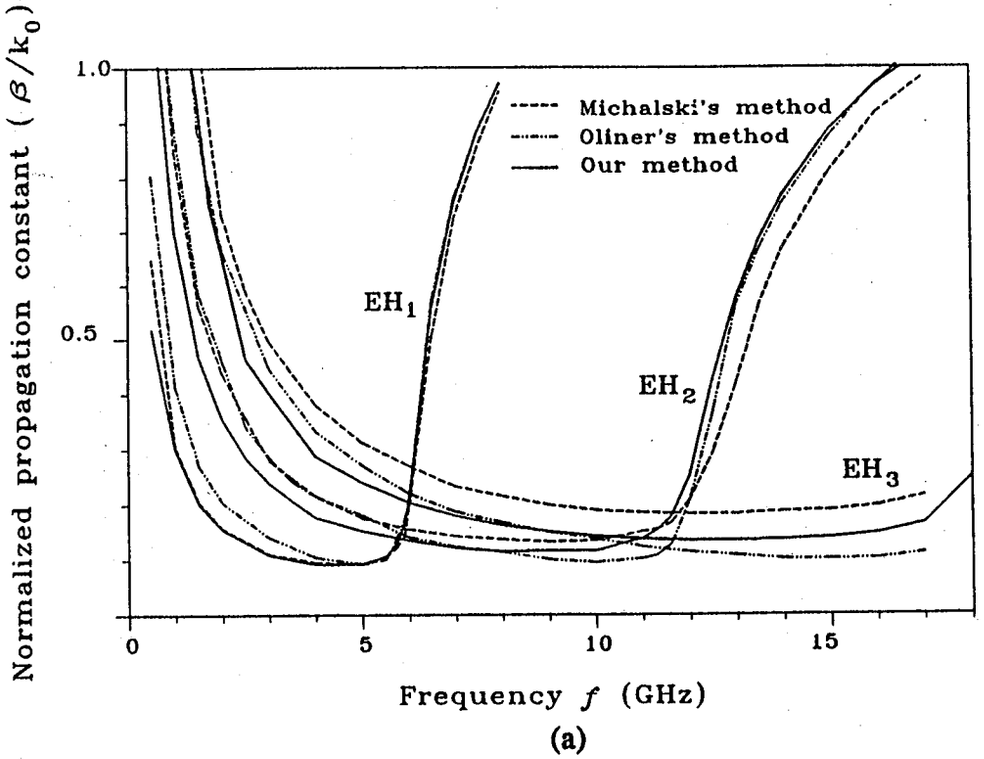

Fig. 6. Dispersion curves for the first three higher order modes of an microstrip structure shown in this figure. (a) Phase constants. (b) Attenuation constants.

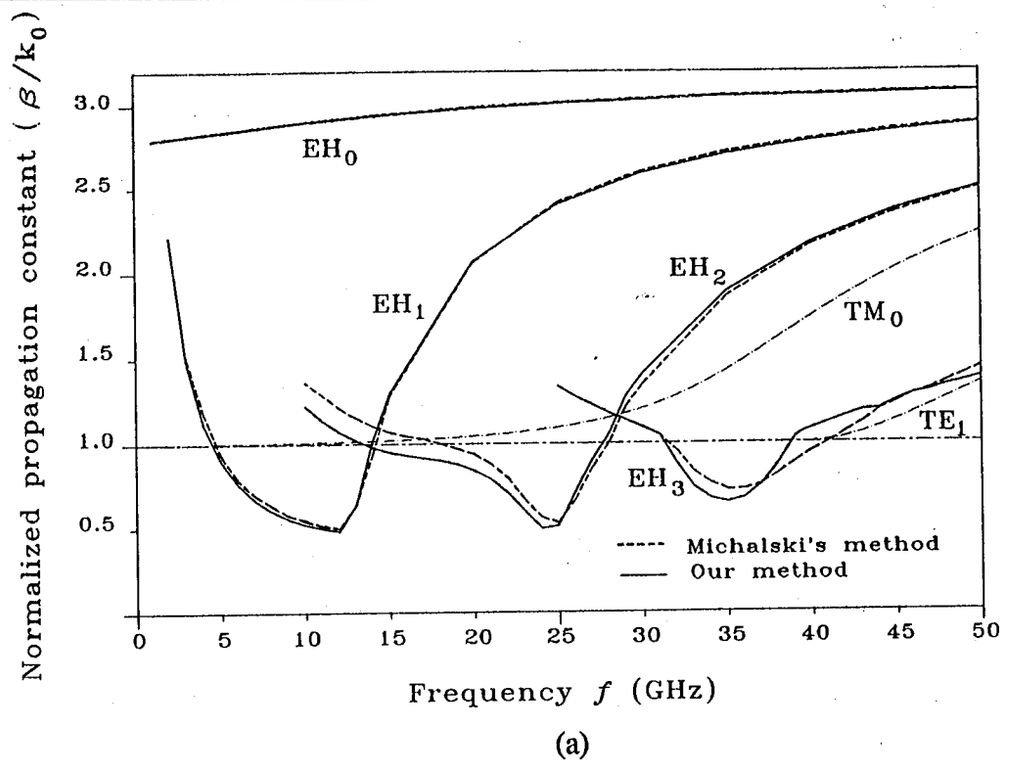

Fig. 7. Dispersion curves for the fundamental mode and the first three higher order modes of an microstrip geometry shown in this figure. (a) Phase constants. (b) Attenuation constants.

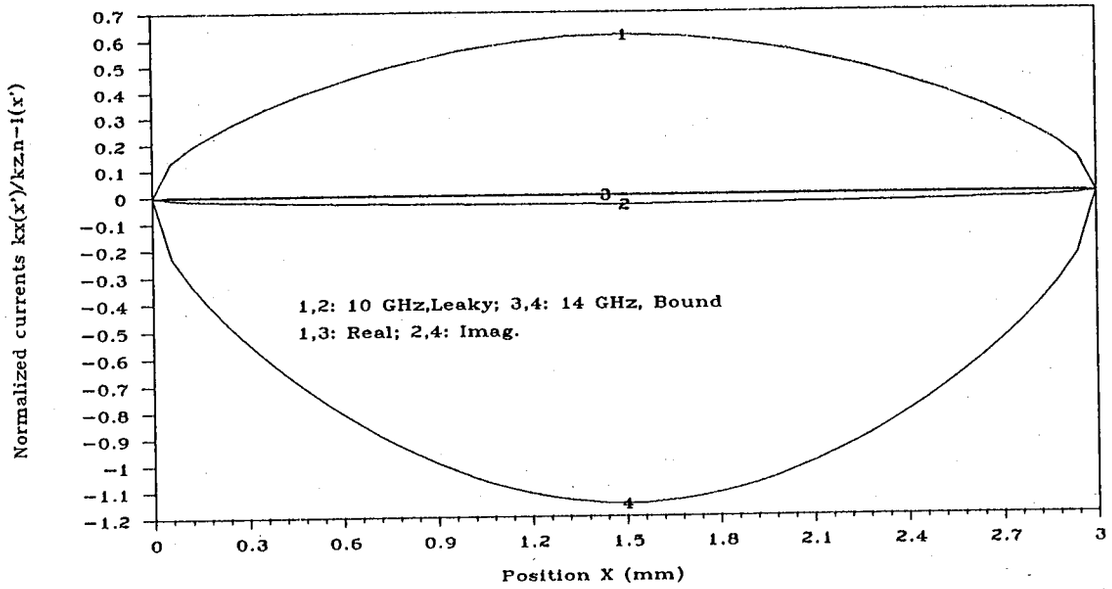

(a)

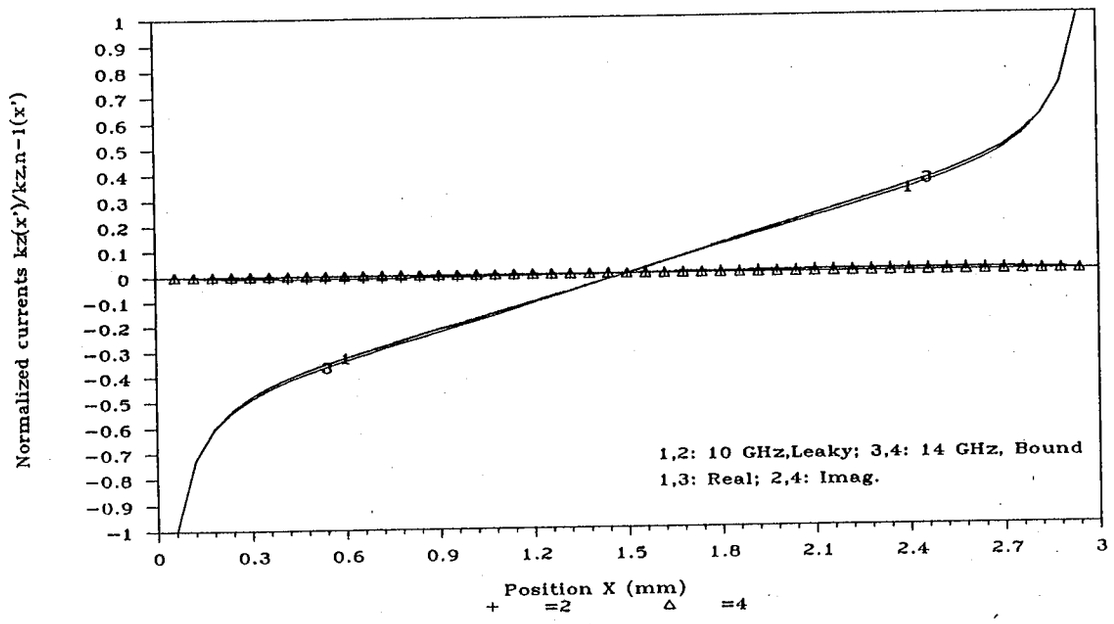

(b)

Fig. 8. (a) Transverse and (b) longitudinal current distributions of the first higher order mode of the microstrip line shown in Fig. 7.

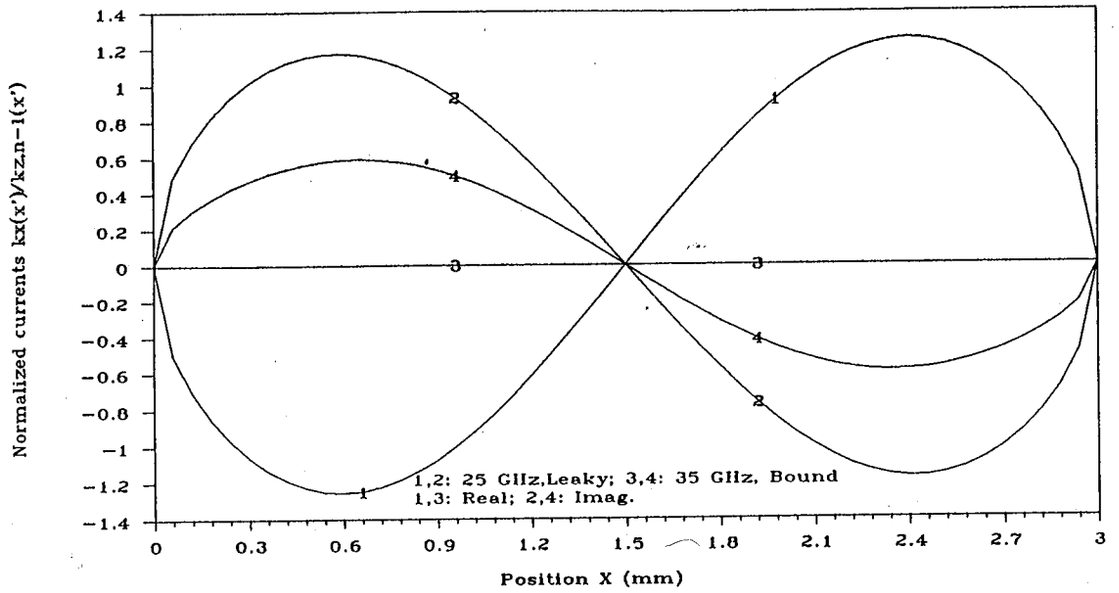

(a)

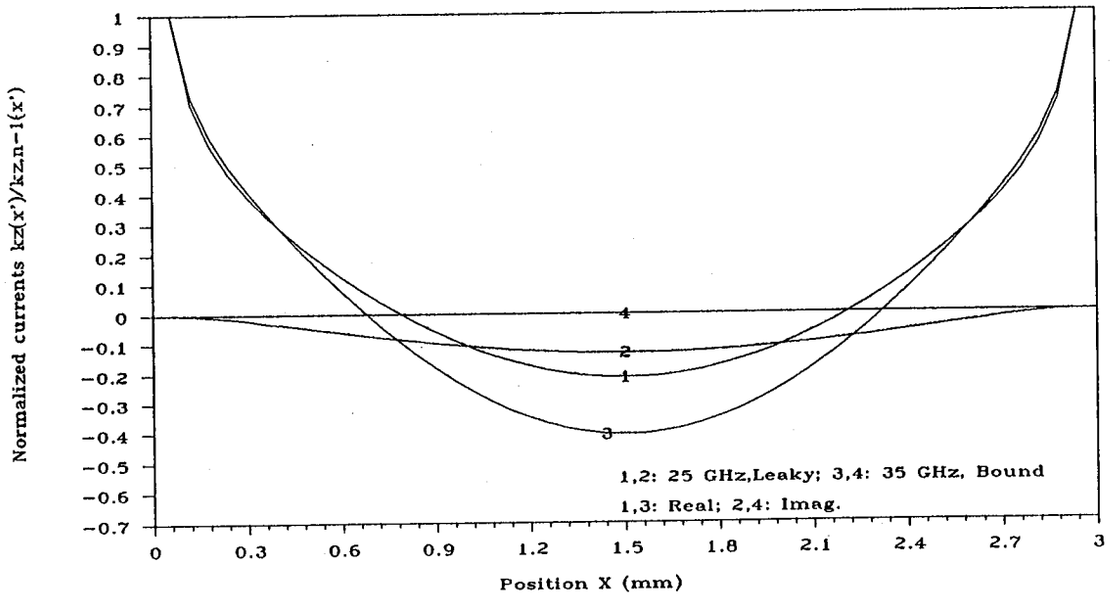

(b)

Fig. 9. (a) Transverse and (b) longitudinal current distributions of the second higher order mode of the microstrip line shown in Fig. 7.

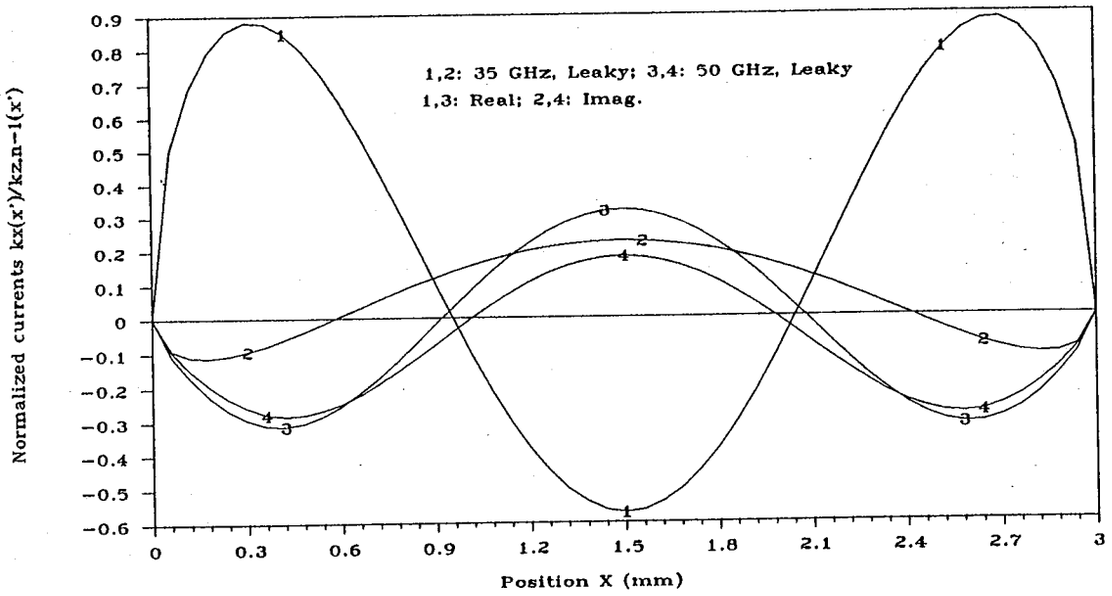

(a)

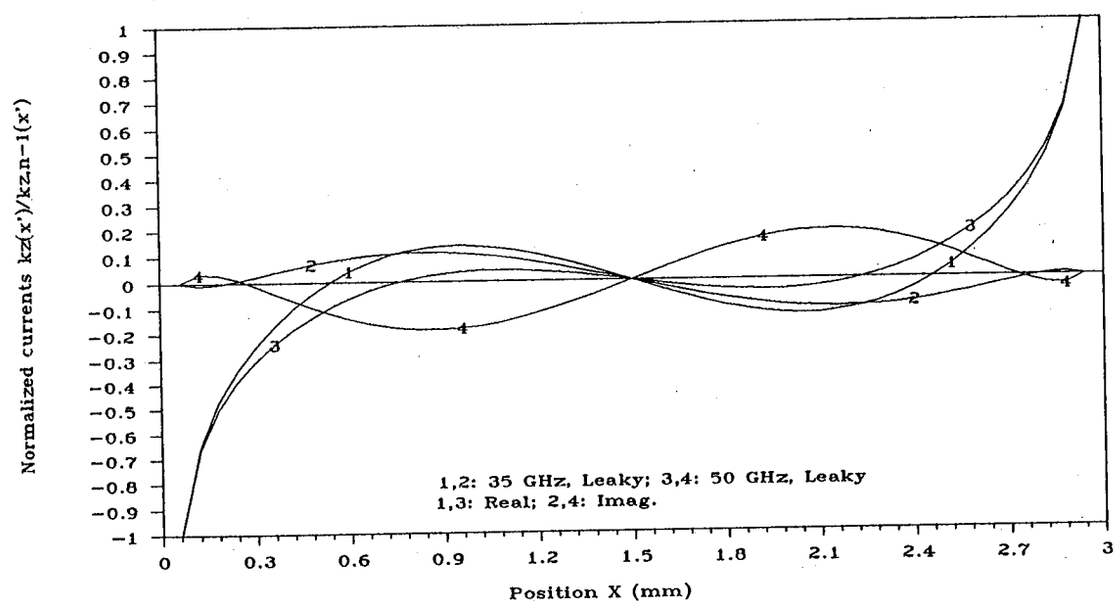

(b)

Fig. 10. (a) Transverse and (b) longitudinal current distributions of the third higher order mode of the microstrip line shown in Fig. 7.

微帶傳輸線洩漏模態之EFIE法解析

李清和 *

摘　　要

近來，由於高模態洩漏區的發現，使研究人員對於微帶傳輸線之傳播特性重新燃起興趣。與微帶傳輸線主模態EH_0不同者，高模態具有三個不同特性之傳播常數區域。本文即在利用一新近發展出來之微帶傳輸線積分方程來解析此三區域之傳播特性，藉由公式中頻域變數在複平面上之分支點與表面波極點之位置，此積分方程提供吾人有關微帶傳輸線上三個不同傳播區特性之清晰概念。文中並以符合微帶傳輸線邊界條件之全域型基底函數MoM法來求模態傳播常數及電流分佈之數值解。與其他使用不同方法之研究者所得結果比較，本研究所得之解與之相當吻合。

* 國立彰化師範大學 工業教育學系 副教授